DEVELOPMENT OF LOW TEMPERATURE SILICON NITRIDE AND SILICON DIOXIDE FILMS BY INDUCTIVELY-COUPLED PLASMA CHEMICAL VAPOR DEPOSITION

J. W. Lee*, K. D. Mackenzie*, D. Johnson*, S. J. Pearton**, F. Ren*** and J. N. Sasserath*
* Plasma-Therm Inc., St. Petersburg, FL 33716
** Dept. of Materials Sci. Eng., University of Florida, Gainesville FL 32611
***Dept. of Chemical Eng., University of Florida, Gainesville FL 32611

ABSTRACT

High-density plasma technology is becoming increasingly attractive for the deposition of dielectric films such as silicon nitride and silicon dioxide. In particular, inductively-coupled plasma chemical vapor deposition (ICPCVD) offers a great advantage for low temperature processing over plasma-enhanced chemical vapor deposition (PECVD) for a range of devices including compound semiconductors. In this paper, the development of low temperature (< 200 °C) silicon nitride and silicon dioxide films utilizing ICP technology will be discussed. The material properties of these films have been investigated as a function of ICP source power, rf chuck power, chamber pressure, gas chemistry, and temperature. The ICPCVD films will be compared to PECVD films in terms of wet etch rate, stress, and other film characteristics. Two different gas chemistries, $SiH_4/N_2/Ar$ and $SiH_4/NH_3/He$, were explored for the deposition of ICPCVD silicon nitride. The ICPCVD silicon dioxide films were prepared from $SiH_4/O_2/Ar$. The wet etch rates of both silicon nitride and silicon dioxide films are significantly lower than films prepared by conventional PECVD. This implies that ICPCVD films prepared at these low temperatures are of higher quality. The advanced ICPCVD technology can also be used for efficient void-free filling of high aspect ratio (3:1) sub-micron trenches.

INTRODUCTION

There is a growing interest in high-density plasma processing in both the semiconductor and the magnetic thin film head industry [1-7]. In particular, much research has been conducted on dry etching with inductively coupled plasma (ICP) sources because they may provide advanced processes for pattern transfer [8-10]. A lot of research has been reported for dielectric film deposition using remote or high-density plasmas [11-14]. However, there is relatively little work on deposition technology for dielectric materials using ICP [15,16]. Using an ICP source, we explored high-density plasma ($>10^{11}$ cm^{-3}) chemical vapor deposition (HDPCVD) of SiN_x and SiO_2. In comparing HDPCVD technology with conventional PECVD, some potential advantages are lower hydrogen content films, higher quality films at lower process temperatures (< 200 °C), void-free gap filling of high aspect ratio features, and self-planarization. Low temperature SiN_x film deposition of low hydrogen content by HDPCVD is of special interest for cap and capacitor layers in III-V semiconductor devices [17-19]. Due to the relatively low dissociation efficiency of N_2, typical process recipes for SiN_x deposition by PECVD use NH_3 as the source of nitrogen. Therefore, some portion of hydrogen incorporation from NH_3 in deposited SiN_x films is inevitable. However, HDPCVD technology enables us to deposit SiN_x with a NH_3-free recipe because high-density plasma sources have typically one order of magnitude higher ion dissociation efficiency (i.e. ~0.1 % for PECVD and ~1 % for HDPCVD).

Some advantages of an ICP source over other types of high-density sources include easier scale up, advanced automatic tuning for the source, and lower cost of ownership. In addition, with a hybrid ICP configuration, such as used in this work, it is possible through the addition of rf power to the wafer chuck, to control ion flux and ion energy independently. This expands the applications for dielectric film deposition by ICP. For example, gap-filling techniques require simultaneous high ion bombardment by an inert gas, such as Ar, during deposition to prevent void formation. To achieve high ion bombardment, high ion energy can be induced by controlling the rf power on the wafer chuck in HDPCVD without change to the ion density in the source. In PECVD, that approach is not feasible and alternating sequences of deposition and sputter etch are usually required. This requires extra steps and more process time. For damage sensitive devices, such as the high electron mobility transistor (HEMT), it is essential to use a very low ion energy process because ion energy is a major factor causing ion damage to the device [20]. With HDPCVD, the ion energy can be reduced to minimize damage of the devices. The process pressures for PECVD and HDPCVD are quite different. More than 500 mTorr is common for PECVD. The pressure range of HDPCVD is 1 to 30 mTorr. We will report on the effect of rf chuck power and pressure for SiN_x films deposited by HDPCVD with an ICP source.

EXPERIMENTAL

Both SiN_x and SiO_2 films were deposited in a Plasma-Therm HDPCVD Versalock system on 4” Si wafers. Figure 1 shows a schematic of the ICP chamber configuration. The load module of the system can handle up to about 50 wafers at a time. For the SiN_x deposition, two different gas chemistries, $SiH_4/N_2/Ar$ and $SiH_4/NH_3/He$, were explored. A gas chemistry of $SiH_4/O_2/Ar$ was used for the SiO_2 film deposition. Electronic mass flow controllers regulated all gas flows. The SiH_4 was fed through a lower gas ring (gas inlet 2). All other gases entered the chamber via a showerhead in the ICP source (gas inlet 1). The process chamber is a hybrid configuration consisting of an inductively coupled plasma (ICP) source and an rf powered wafer chuck. An oil recirculating heat exchanger connected to the chuck controls the wafer temperature. Helium backside cooling of the wafer is used for efficient heat transfer. For this work, the ICP source power and chuck temperature were fixed at 800 W and 150 °C respectively. The rf chuck power and chamber pressure were varied from 25 to 150 W and 1 to 20 mTorr, respectively.

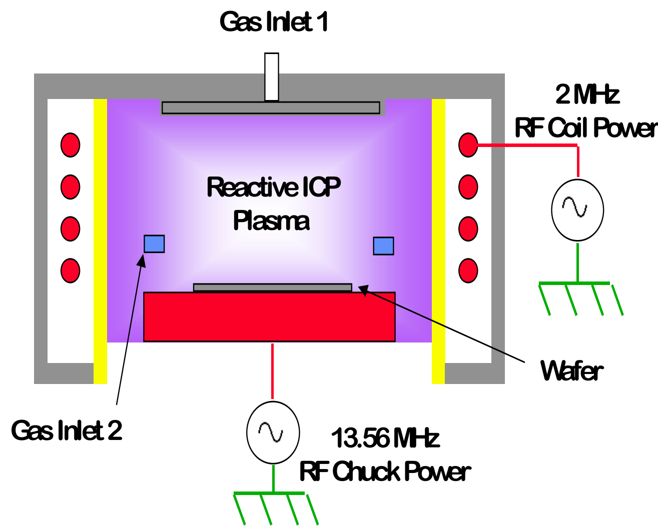

Figure 1. Schematic of the ICP chamber.

Langmuir probe measurements of ICP Ar plasmas were used to determine the ion density characteristics of the process chamber. In-situ optical emission spectroscopy (OES) was also used to characterize the ICP $SiH_4/N_2/Ar$ plasmas.

Deposition rate and uniformity were determined by a NanoSpec model 4150 metrology system. Refractive index measurements were made on a Gaertner model L116D-PC

ellipsometer. Film stress measurements were done with a Tencor model P-2 profilometer. A buffered oxide etch (BOE) solution of 7:1 NH_4: HF was used for the wet-etch rate measurements.

RESULTS AND DISCUSSION

ICPCVD Plasma Characterization

Figure 2 shows ion density and negatively induced dc bias as a function of ICP source power and rf chuck power for Ar plasmas at a fixed pressure of 10 mTorr. These data were obtained from a design of experiment simulation, which we developed with experimental data obtained on the ICP process chamber. As shown in Figure 2 (a), the ion density of the Ar plasma can be controlled by ICP source power and is almost independent of rf chuck power. The Ar ion density is about 2×10^{11} cm^{-3} with 800 W ICP power, 20 sccm Ar, 10 mTorr chamber pressure, and 100 W rf chuck power. As illustrated in Figure 2 (b), it was also found that the dc bias on the chuck was a strong function of ICP source power and rf chuck power. The dc bias, in other words, ion energy increased with rf chuck power and decreased with ICP source power.

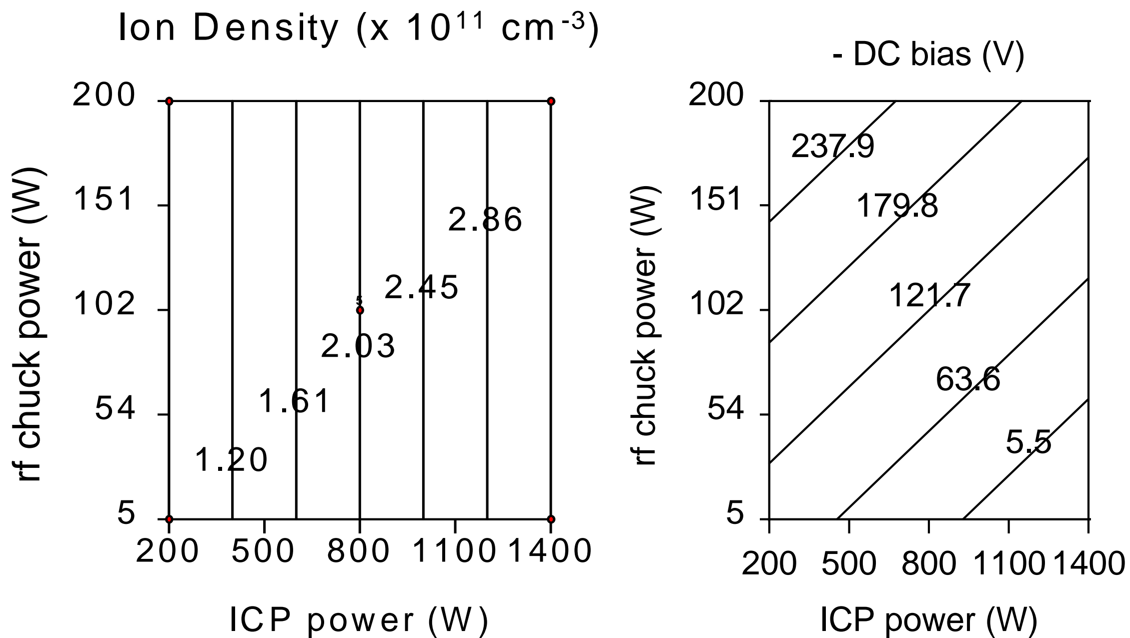

Figure 2. Ion density (a) and negatively induced dc bias (b) as a function of rf chuck power in an ICP chamber for Ar plasmas.

Silicon Nitride: Optical Emission Spectra

In Figure 3, a typical optical emission spectrum (OES) is presented for an ICP $SiH_4/N_2/Ar$ plasma. This spectrum was recorded during a SiN_x deposition. All N_2, SiH, H_2, and Ar related peaks were identified. Figure 4 shows more detailed OES data taken at different rf powers. Many N_2 related peaks were detected between 300 and 400 nm. A N_2^+ peak is also

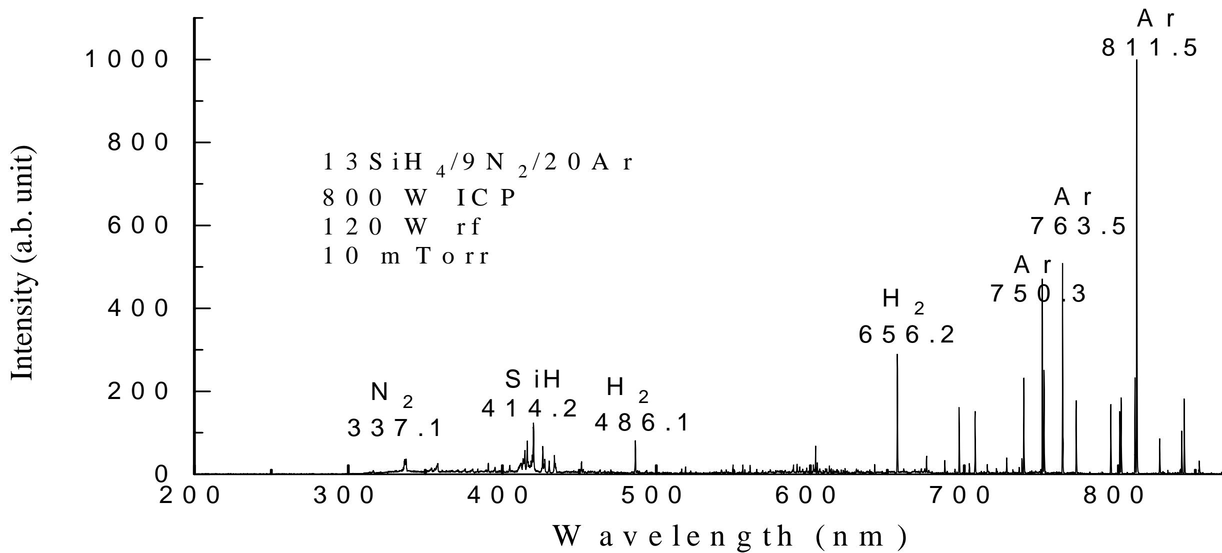

Figure 3. Optical emission spectrum of an ICP $SiH_4/N_2/Ar$ plasma at 800 W ICP, 120 W rf, and 10 mTorr.

noticed at 391.4 nm. A SiH and two H_2 peaks are observed at 414.2, 486.1 and 656.2 nm, respectively. The peak intensities of both SiH and H_2 increased with increasing rf power.

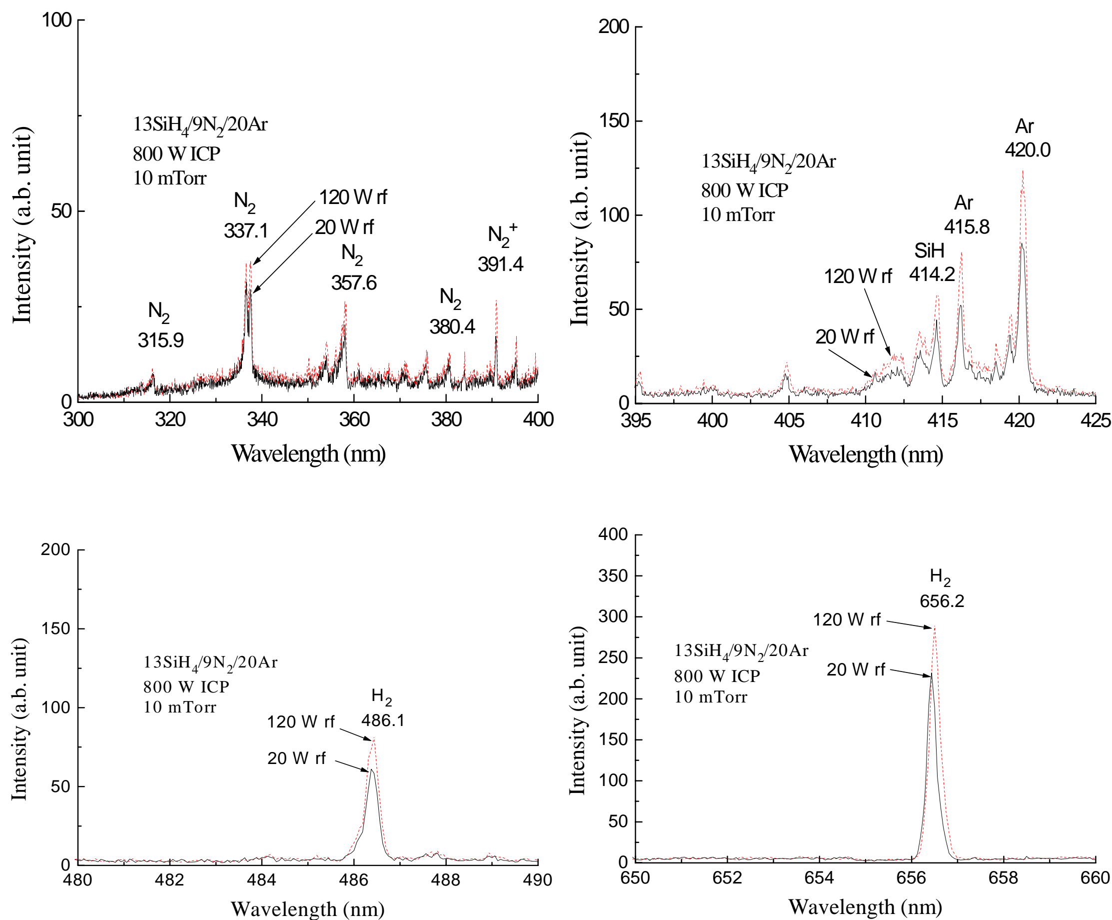

Figure 4. Detailed optical emission spectra for an ICP $SiH_4/N_2/Ar$ plasma for rf chuck powers of 20 and 120 W. The ICP power and pressure were 800 W ICP and 10 mTorr, respectively.

Silicon Nitride: Film Properties

1. Results for $SiH_4/N_2/Ar$

In Figure 5, the dependence of deposition rate on rf chuck power is shown. The deposition rate decreases with increasing rf chuck power. At high rf power, it is expected that more ion bombardment during deposition will occur. High rf power increases the dc bias and consequently the ion energies of the bombarding species, e.g. Ar^+ and N_2^+, will increase. This will enhance the sputtering of Si and N reactive neutrals before and during the formation of the SiN_x film. This accounts for the observed reduction in deposition rate with rf power. The typical deposition rate was in the range 400 to 600 Å/min.

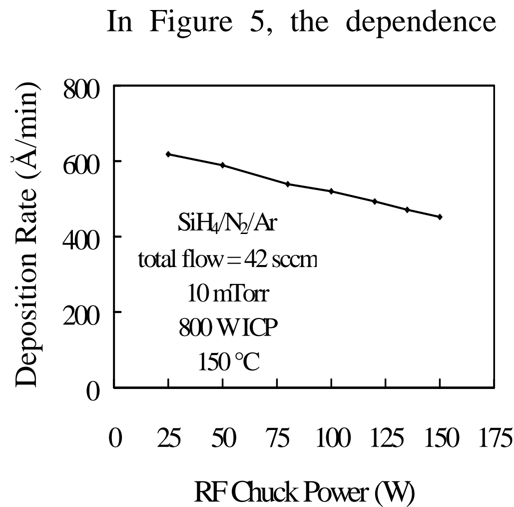

Figure 5. SiN_x deposition rate as a function of rf chuck power.

Figures 6 and 7 show the variation of refractive index and BOE rate with rf chuck power. At 25 W rf chuck power, a refractive index of 1.95 was achieved. The combination of decrease of deposition rate and BOE rate, and increase of refractive index with rf chuck power indicates that deposited films become Si-rich and densified as the rf chuck power is increased. The density, ρ may be calculated from the following equation:

$$\rho = (28[Si] + 14[N])/A \quad (1)$$

where [Si] is atomic concentration of Si, [N] is atomic concentration of N, and A is Avogadro's number.

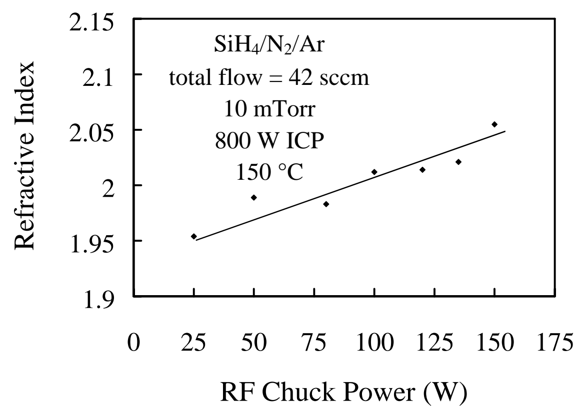

Figure 6. Refractive index of ICPCVD SiN_x as a function of rf chuck power.

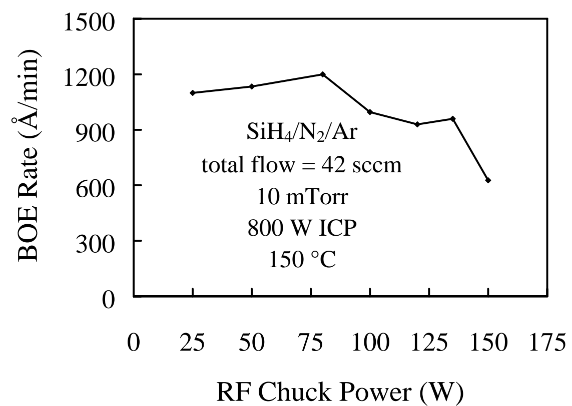

Figure 7. BOE rate of ICPCVD SiN_x as a function of rf chuck power.

One possible explanation for the increase of refractive index with rf power is that the dissociation of SiH_4 into reactive neutrals in the $SiH_4/N_2/Ar$ plasma increased relative to that of N_2 with rf chuck power (in other words, ion energy). Another possible explanation is that high rf power brings more Si-related species than N to participate in the film growth. Table I shows the dissociation energy of related diatomic molecules for SiN_x deposition. Notice that the N-N bond has a much higher bond strength (945.33 kJ/mol) than that of Si-H ($\leq$ 299.2 kJ/mol). Dissociation of N_2 requires more energy than that of SiH_4. All of this data suggests that more SiH_4 species are brought to the substrate than N_2 with increase of rf chuck power.

Table I. Dissociation energies of diatomic molecules.

Bond	Dissociation Energy at RT (kJ/mol)
Si-H	≤ 299.2
N-H	≤ 339
N-N	945.33
H-H	435.99

It is worthwhile commenting further on the BOE data presented in Figure 7. Considering the low deposition temperature of 150 °C, the typical BOE rate of 1000 Å/min is very low. At 150 °C, the BOE rate of PECVD SiN_x is greater than 5,000 Å/min. This implies that the ICPCVD SiN_x films are denser and contain less hydrogen [21].

As indicated in Figure 8, the stress of all ICPCVD SiN_x films prepared from $SiH_4/N_2/Ar$ was compressive. At 25 W rf chuck power, the film stress was as high as 900 MPa. Raising the rf chuck power lowers the film stress. A stress of 300 MPa is achieved at 120 W. Film stress of less than 500 MPa is acceptable for many applications. We speculate that incorporated hydrogen relieves the stress in the SiN_x film, although the correlation with rf chuck power is not fully understood. In PECVD, the film stress increases with rf power regardless of whether it is compressive or tensile. This is diametrically opposite to the current observations with ICPCVD.

Figure 9 shows deposition uniformity versus rf chuck power. The typical uniformity is less than 4 %. The uniformity becomes somewhat worse as the rf chuck power is increased. It was observed that the center of the deposited films was thicker than edge of the wafer.

As presented in Figures 10 and 11, raising the chamber pressure increased both the deposition rate and refractive index. The deposition rate increases from 350 Å/min at 1mTorr to

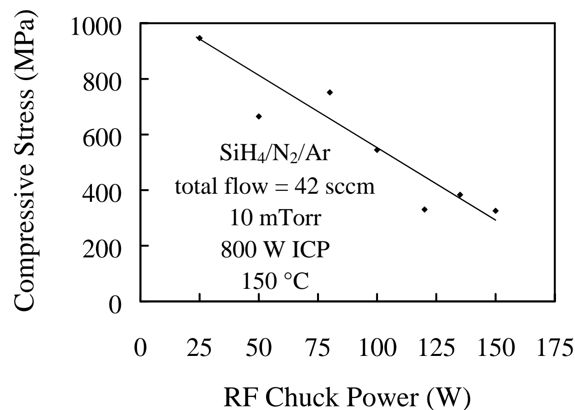

Figure 8. Compressive stress of ICPCVD SiN_x as a function of rf chuck power.

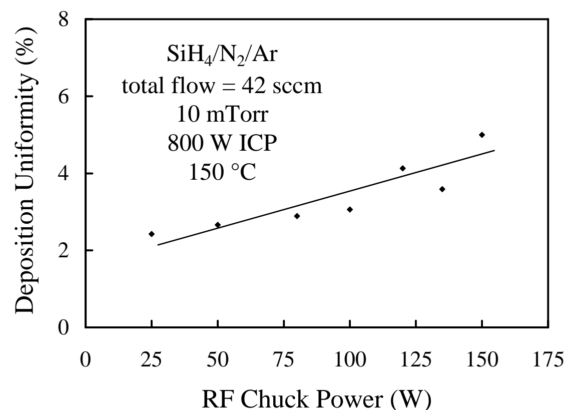

Figure 9. Deposition uniformity of ICPCVD SiN_x as a function of rf chuck power.

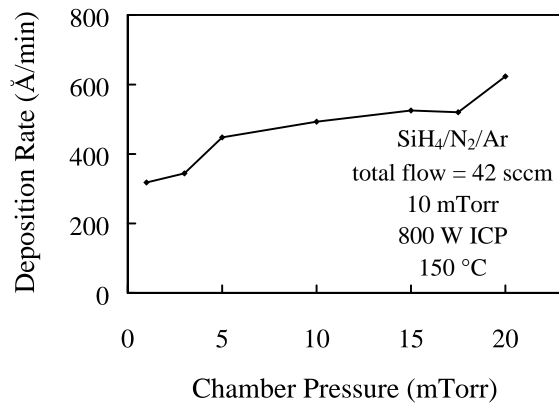

Figure 10. Deposition rate of ICPCVD SiN_x as a function of chamber pressure.

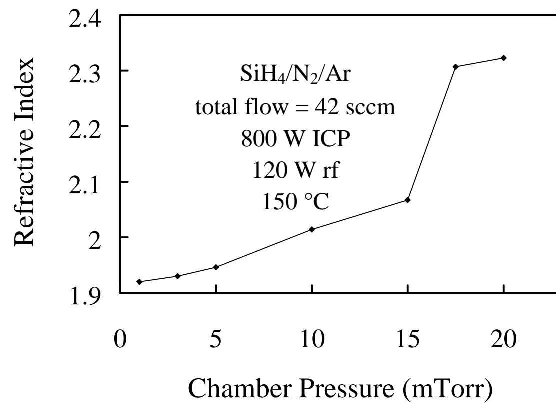

Figure 11. Refractive index of ICPCVD SiN_x as a function of chamber pressure.

600 Å/min at 20 mTorr. Over this pressure range, the refractive index increases from 1.92 to 2.32. As shown in Figure 12, the BOE rate decreases from 1200 to 400 Å/min as the pressure is increased. At high pressure, the residence time of gas species increases by the equation:

$$\tau = PV/Q \tag{2}$$

where τ, P, V, and Q are the residence time, pressure, volume, and throughput, respectively. With longer residence time and higher Ar ion density at high chamber pressure, more SiH_4 may be dissociated into neutrals, which will be incorporated in the films and cause a Si-rich composition at high pressure. It is well known that increased refractive index with Si-rich composition reduces the BOE rate of the films.

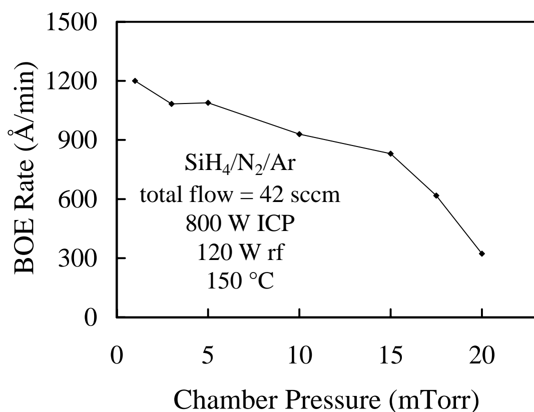

Figure 12. BOE rate of ICPCVD SiN_x as a function of chamber pressure.

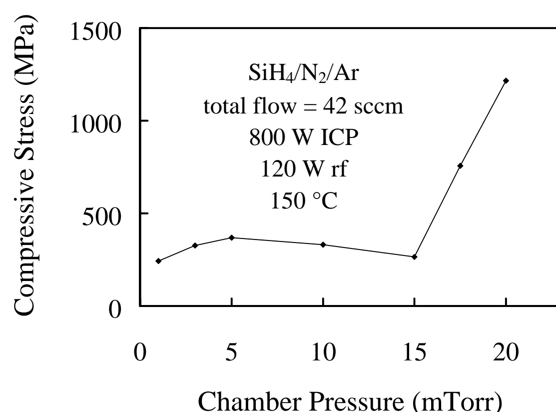

Figure 13. Compressive stress of ICPCVD SiN_x as a function of chamber pressure.

As shown in Figure13, the stress of the deposited films is constant at about 400 MPa, compressive over the pressure range of 1 to 15 mTorr. However, at higher pressure (> 15 mTorr), stress increased rapidly and reached 1300 MPa at 20 mTorr.

1. Results for $SiH_4/NH_3/He$

ICPCVD SiN_x deposition from $SiH_4/NH_3/He$ was also investigated. Table II summarizes some of data obtained. The process conditions were 800 W ICP power, 30 W rf chuck power, 10 mTorr, and 150°C.

Table II. Characteristics of ICPCVD SiN_x with $SiH_4/NH_3/He$.

Refractive Index	2.0	BOE Rate	1200 Å/min
Deposition Rate	300 Å/min	Uniformity	+/- 2.5 %
Film Stress	200 MPa, (compressive)		

Deposition rate was not a strong function of rf chuck power (Figure 14) while stress was controlled by rf chuck power (Figure 15). The film stress was compressive at low rf chuck power and it became tensile with more rf chuck power.

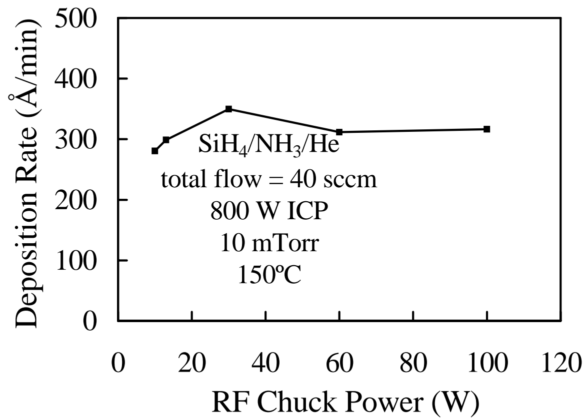

Figure 14. Deposition rate of ICPCVD SiN_x as a function of rf chuck power.

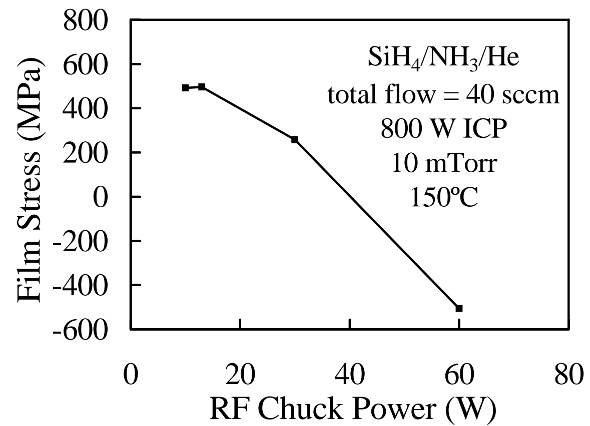

Figure 15. Compressive stress of ICPCVD SiN_x as a function of rf chuck power.

Silicon Dioxide: Gap Filling

The application of ICPCVD SiO_2 for void-free filling of 1 μm gap features was investigated. Table III summarizes some of the main properties of these films.

Table III. Characteristics of ICPCVD SiO_2 film.

Gas Chemistry	$SiH_4/O_2/Ar$
Deposition Rate	~1000 Å/min
Film Stress	300 MPa, (compressive)
Refractive Index	1.46

Figure 16 shows an SEM micrograph of a gap-filled Si trench. The aspect ratio of the trench was about 3:1. Notice that there is no void after gap filling is completed. A similar technique was applied on an electroplated metal which had an irregular shaped sidewall. Figure 17 shows self-planarization after gap filling. Note that there were small voids after the process was completed. The origin of the void is from the irregularity of sidewall at the bottom of the trench. As illustrated in Figure 18, with modified process conditions to compensate for the

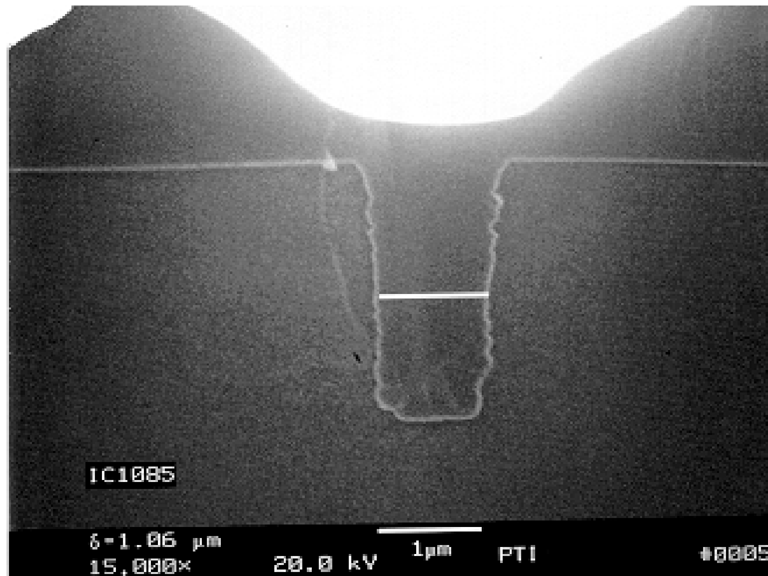

Figure 16. SEM micrograph showing a Si trench filled with ICPCVD SiO_2.

sidewall problem of the control samples, the trench can be filled with ICPCVD SiO_2 without any void. Further processing would bring self-planarization after gap filling.

SUMMARY AND CONCLUSIONS

We investigated low temperature deposition (150 °C) of ICPCVD SiN_x prepared from $SiH_4/N_2/Ar$ and $SiH_4/NH_3/He$. For SiN_x films prepared from $SiH_4/N_2/Ar$, rf chuck power increased refractive index and deposition uniformity while it decreased deposition rate, stress, and BOE rate. Increasing rf chuck power may bring more Si species than N species to the wafer surface leading to Si-rich films. Raising the chamber pressure resulted in higher deposition rate, refractive index, and film stress. The BOE rate of ICPCVD SiN_x, prepared from either $SiH_4/N_2/Ar$ or $SiH_4/NH_3/He$, is much lower compared to PECVD SiN_x deposited at the same low temperature. This implies that the ICPCVD SiN_x films are denser and contain less hydrogen. An ICPCVD SiN_x process for adjustable film stress was demonstrated using $SiH_4/NH_3/He$.

ICPCVD SiO_2 films were prepared from $SiH_4/O_2/Ar$. Void-free gap filling of high aspect ratio trench was demonstrated with ICPCVD SiO_2.

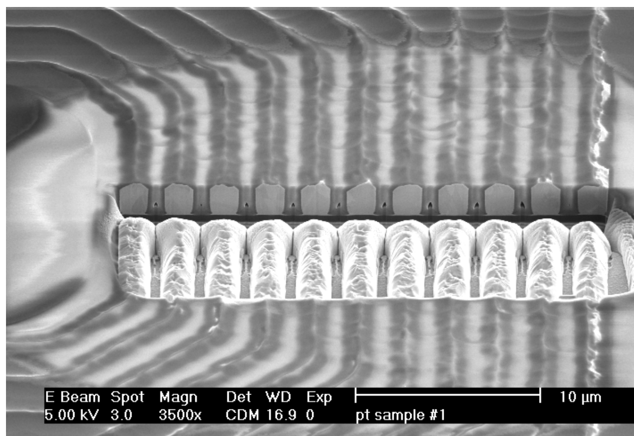

Figure 17. Gap-filled and self-planarized SiO_2 on metal coils by ICPCVD.

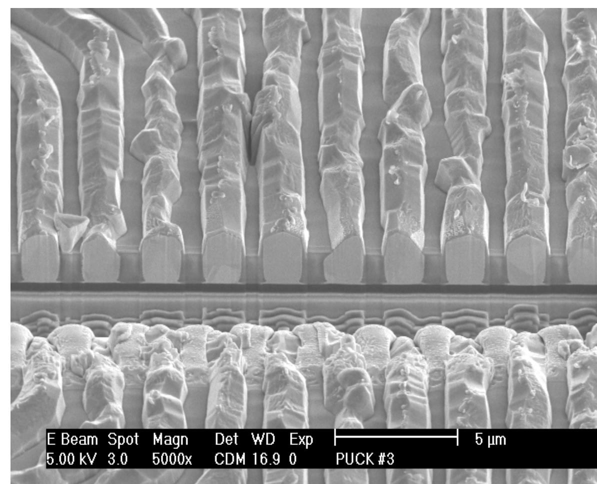

Figure 18. Partially gap-filled metal coils by ICPCVD SiO_2. No voids are evident. The SiO_2 film is planarized.

In conclusion, high-density ICPCVD technology clearly has many advantages compared to PECVD for dielectric film deposition in a broad range of advanced processes for electronic device fabrication, especially at low temperatures.

ACKNOWLEDGMENTS

The authors appreciate Dr. J. Donohue, Mr. R. Westerman, and Mr. Wei Pen for fruitful discussions and assistance. We also thank Mr. R. McAfee and Mr. L. Heckerd for their technical support. The work at UF is partially supported by a DOD MURI, monitored by AFOSR (H. C. DeLong), contract no. F49620-96-1-0026.

REFERENCES

1. C. Constantine, C. Barratt, S. J. Pearton, F. Ren and J. R. Lothian, Appl. Phys. Lett. **61**, 2899 (1992).

2. J. W. Lee, H. Cho, C. Hays, C. R. Abernathy, S. J. Pearton, R. J. Shul and G. A. Vawter and H. Han, IEEE J. of Selected Topics in Quantum Electronics, **4**, 557 (1998).

3. F. Ren, J. W. Lee, C. R. Abernathy, S. J. Pearton, C. Constantine, C. Barratt and R. J. Shul, J. Vac. Sci. Technol. B **15**, 983 (1997).

4. S. J. Pearton, J. W. Lee, E. S. Lambers, J. R. Mileham, C. R. Abernathy, W. S. Hobson and F. Ren, J. Vac. Sci. Technol. B **14**, 118 (1996).

5. S. Thomas III, K. K. Ko and S. W. Pang, J. Vac. Sci. Technol. A **13**, 894 (1994).

6. K. B. Jung, J. Hong, H. Cho, S. Onishi, D. Johnson, Y. D. Park, J. R. Childress, and S. J. Pearton, J. Vac. Sci. Technol. A **17**, 535 (1999).

7. R. J. Shul, G. B. McClellan, R. D. Briggs, D. J. Rieger, S. J. Pearton, C. R. Abernathy, J. W. Lee, C. Constantine and C. Barratt, J. Vac. Sci. Technol. A **15**, 633 (1997).

8. J. W. Lee, E. S. Lambers, C. R. Abernathy, S. J. Pearton, R. J. Shul, F. Ren, W. S. Hobson and C. Constantine, Solid-State Electron. 42 A65-A73 (1998).

9. R. J. Shul, C. G. Wilson, M. M. Bridges, J. Han, J. W. Lee, S. J. Pearton, C. R. Abernathy, J. D. MacKenzie, L. Zhang and L. F. Lester, J. Vac. Sci. Technol. A **16**, 1621 (1998).

10. F. Ren, J. W. Lee, C. R. Abernathy, R. J. Shul, C. Constantine and C. Barratt, Semicond. Sci. Tech. **12**, 1154 (1997).

11. G. Lucovsky, P. D. Richard, D. V. Tsu, S. Y. Lin and R. J. Markunas, J. Vac. Sci. Technol. A **4**, 681 (1986).

12. C. B. Labelle, S. J. Limb and K. K. Gleason, J. Appl. Phys. **82**, 1784 (1997).

13. S. J. Limb, C. B. Labelle, K. K. Gleason, D. J. Edell and E. F. Gleason Appl. Phys. Lett. **68**, 2810 (996).

14. M. Lapeyrade, M. P. Besland, C. Meva'a, A. Sibai and G. Hollinger, J. Vac. Sci. Technol. A **17**, 433 (1999).

15. Y. B. Hahn, J. W. Lee, K. D. Mackenzie, D. Johnson, S. J. Pearton and F. Ren, Solid-State Electron. **42**, 2017 (1998).

16. Y. B. Hahn, J. W. Lee, K. D. Mackenzie, D. Johnson, D. Hays, C. R. Abernathy and S. J. Pearton, Electrochemical and Solid-State Lett. **1**, 230 (1998).

17. J. W. Lee, K. D. Mackenzie, D. Johnson, R. J. Shul, S. J. Pearton, C. R. Abernathy and F. Ren, Solid-State Electron. **42**, 1031 (1998).

18. J. W. Lee, C. R. Abernathy, S. J. Pearton, F. Ren, R. J. Shul, C. Constantine and C. Barratt, Solid-State Electron. **41**, 829 (1997).

19. F. Ren, J. W. Lee, C. R. Abernathy; S. J. Pearton, R. J. Shul, C. Constantine and C. Barratt, Semicond. Sci. Technol. **12**, 1154 (1997).

20. J. W. Lee, K. D. Mackenzie, D. Johnson, R. J. Shul, S. J. Pearton, C. R. Abernathy and F. Ren, Solid-State Electron. **42**, 1021 (1998).

21. J. Kanicki, Mat. Res. Soc. Symp. Proc., **118**, 671 (1988).